

PARAMETERIZATION OF MOBILIZATION AND TRANSPORT OF SAND-DUST DURING BLACK STORM AND MESOSCALE NUMERICAL EXPERIMENTS *

Liu Chuntao (刘春涛) and Cheng Linsheng (程麟生)

Department of Atmospheric Sciences, Lanzhou University, Lanzhou 730000

Received March 20, 1998

ABSTRACT

The typical black storms or sand-dust storms in the northwestern China are generated and developed through an interaction between the specific large scale circulation pattern and mesoscale systems. The passing by/over a huge sand-abundant desert of a strong cold front with intensive frontal zone at mid and lower levels is a necessary condition for the formation and development of a black storm or a severe sand-dust storm. In order to investigate the mechanism of the sand-dust mobilization, transport and sedimentation during the black or sand-dust storms, a parameterization scheme of sand-dust source-sink terms and an equation of transport for the sand-dust were proposed and incorporated into the MM4 mesoscale model. The modified MM4 model was applied to the "May 1993" black storm case and succeeded in reproducing the evolution of the weather systems associated with the black-storm, the sand-dust concentration at surface layer and its vertical distribution, and the sand-dust sedimentation and transport. Our results show that the numerical simulating method by using a mesoscale model, with inclusion of an equation of the sand-dust transport and a parameterization scheme of the sand-dust source-sink terms, is a promising approach to study the mechanism for sand-dust mobilization, transport and sedimentation during a sand-dust storm event.

Key words: black storm, mobilization and transport of sand-dust, parameterization of sand-dust source and sink terms, numerical simulation

I. INTRODUCTION

An extraordinary severe storm with huge sand-dust outbreak occurred in the desert-gobi areas and its eastern edge in the northwestern China during the period of 4–6 May 1993 ("93.5"). It swept 18 cities and 72 counties of four Provinces and Autonomous Regions from west to east, including the desert-gobi of the northern and eastern parts in Xinjiang Uygur Autonomous Region, Hexi Corridor of Gansu Province, Ningxia plain, Badain Jaran Desert and Tengger Desert in Inner Mongolia Autonomous Region. Its average wind speed was 20 m s^{-1} , the maximum wind speed reached 34 m s^{-1} and visibility decreased to zero at Jinchang City when it passed. The disastrous damage occurred at Jinchang City, Yongchang County, Wuwei City and other places. According to the

* This study was supported by the National Natural Science Foundation of China under grant 49475268.

observation, a destructive black storm had been formed in the places as mentioned above (Chen et al. 1993; Yang et al. 1993). This black storm is the severest one since the beginning of meteorological observation in 1927. After "93. 5" black storm, a weather event of severe sand-dust storm with wide coverage occurred again during the period of 5—11 April 1994 ("94. 4") in Gansu, Ningxia, Xinjiang and western region of Inner Mongolia Autonomous Region as well as some parts of Qinghai (Xu 1996). A section of Lanzhou-Xinjiang railway was covered by sand up to 2 m (Huang 1994). These two sand-dust linked disasters caused severe damage to the people's life and property as well as the agriculture and economy in the regions as mentioned above. Thus, it is necessary to study the mechanism of the mobilization, transport, and sedimentation of the sand-dust during the the black storm events.

Because of the likely disastrous consequence of the sand-dust storms, there have been many studies on this subject. Xu et al. (1979) conducted a synoptic analysis on "4. 22" sand-dust storm in Gansu; Iwasaka et al. (1983) studied the transport and scale analysis of "Yellow Sand" case in Asia; Westphal et al. (1988) studied the cases of mobilization and transport of Saharan dust; Karyampudi and Carlson (1988) carried out an analysis of Saharan air layer. Jiang (1995) gave an analysis of generation of "93. 5" black storm by GMS-4 satellite cloud image. Chen et al. (1993) pointed out that ahead of a cold front in company with "93. 5" black storm existed a dry squall line. Cheng et al. (1995) and Cheng and Ma (1996) used the improved mesoscale model to study the developmental structure and formation of "93. 5" black storm, and came to the conclusion that the formation and development of "93. 5" black storm was in close relationship with the generation and quick development of a mesoscale cyclonic vortex in lower troposphere, and the intense cold front associated with the black storm possessed the characteristics of squall line.

Although much research work on the sand-dust/black storms has been done, yet few of them involved the numerical experiments conducted to investigate the genesis and development of the sand-dust/black storm. Therefore, we will attempt to carry out some investigations in this respect. First, we propose a three-dimensional equation of the sand-dust transport and a parameterization scheme of sand-dust mobilization at the surface and its sedimentation and add them to the well-established mesoscale model MM4. Then, based on this modified model, we conduct the control simulations of the sand-dust transport during "May 1993" black storm. We also conduct simulations of the "April 1994" sand-dust storm to further study the general mechanisms responsible for the sand-dust generation and development.

II. BRIEF SYNOPTIC ANALYSIS OF THE "MAY 1993" BLACK STORM

This black storm weather event was mainly caused by the quick invasion of Siberian cold air from northwest to southeast, one part of the cold air moved across over Tianshan Mountain, passed eastern Xinjiang and got into Hexi area, while the black storm was associated with an eastward quickly moved surface cold front with squall line characteristics (Chen et al. 1995; Cheng and Ma 1996). Figure 1 is the regional surface weather map at 1700 BT (Beijing Time, hereafter the same) 5 May (Cheng and Ma

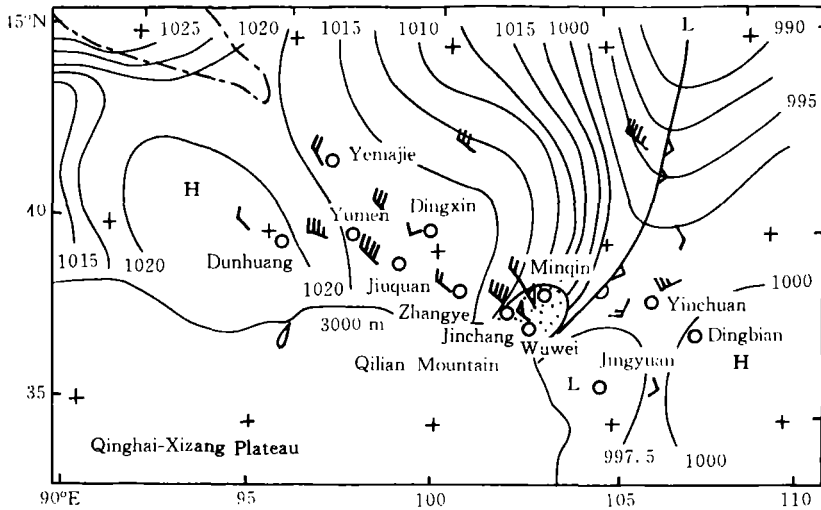


Fig. 1. Regional surface synoptic analysis at 1700 BST 5 May 1993 (The shadow is the black storm area).

1996). The cold front passed by Zhangye at 1400 BT 5 May, and the allobaric gradient on both sides of the cold front was very strong, accompanied by a mesoscale trough and a mesoscale ridge ahead and behind the cold front, respectively (figure omitted). The severe sand-dust storm was formed in the Badain Jaran Desert when the cold front passed by this area, and with the southward move and the intensification of the cold front, the NW wind speed was intensified behind the cold front (the maximum wind speed was reached 34 m s^{-1} at Jinchang City). The sand-dust storm was intensified and became the black storm when it moved into the edge of the Tengger Desert in Zhangye, Jinchang and Minqin regions due to the dry surface and severe wind erosion conditions in these areas.

When black storm passed, not only was the sunlight covered by the sand-dust, but the surface temperature, pressure, wind speed and humidity etc. changed abruptly. Figure 2 shows the variation with time of the main meteorological elements at Jinchang station during May 5, 1993 (Chen et al. 1995). We can see from Fig. 2 the intensive cold front associated with the black storm possesses the character of the squall line.

Figure 3 is the land-use categories of underlying surface in the simulation domain, in which the isoline 9 represents the desert-gobi area. Some large desert areas are marked by the thick lines, including Badain Jaran Desert near 42°N , 100°E , Tengger Desert near 39°N , 102°E , as well as the Kumtag Desert and Qaidam Basin Gobi around 42°N , 92°E . Most of the sand-dust storms in the Northwest China, especially in Hexi area of Gansu are related to these three sand-dust sources.

From the analysis above, it is seen that the formation and development of the "93.5" black storm were not only related to a special circulation pattern and mesoscale circulation system, but also related to the presence of the wide underlying desert surface and the poor environmental conditions. The same conclusion can be drawn with the "April 1994" sand-dust storm case regarding its synoptic background. A detail description is omitted here.

In the next section, we will develop a three-dimensional equation of sand-dust

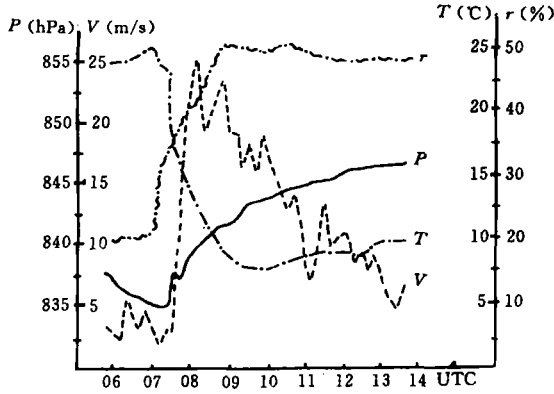


Fig. 2. The variation with time of the surface pressure (*P*), temperature (*T*), relative humidity (*r*), wind speed (*V*) at Jinchang station during the period May 5, 1993.

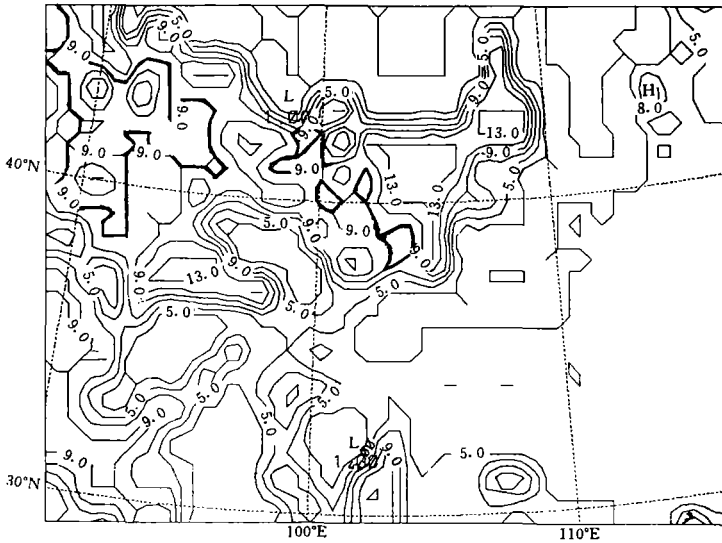


Fig. 3. The land-use categories of underlying surface in the simulation domain (The areas surrounded by the thick lines express the large desert area in the Northwest China).

transport and a parameterization scheme of driving sand-dust mobilization from the surface and sand-dust sedimentation with particle size distribution in the air.

III. TRANSPORT EQUATION OF SAND-DUST AND PARAMETERIZATION OF ITS SOURCE/SINK TERMS

1. Transport Equation of Sand-Dust

Considering that the formation, transport and sinking processes of the sand-dust material are similar to those of the aerosol contaminants, thus we can get a conservative equation of the sand-dust, which is similar to that of aerosol contaminants, as follows:

$$\frac{\partial \chi}{\partial t} = - \mathbf{V} \cdot \nabla \chi + S_{\chi} - D_{\chi} \tag{1}$$

where χ is the concentration of sand-dust, namely, the mass of sand-dust in the unit volume. S_χ and D_χ are source (mobilization) and sink (sedimentation) terms of sand-dust, respectively. After converting Eq. (1) into the σ [$\sigma = \left(\frac{p - p_t}{p_s - p_t} \right)$] coordinates system with Lambert map project and map factor m , we can get

$$\frac{\partial p^* \chi}{\partial t} \textcircled{1} = -m^2 \left(\frac{\partial p^* u \chi / m}{\partial x} \textcircled{2} + \frac{\partial p^* v \chi / m}{\partial y} \right) - \frac{\partial p^* \sigma \chi}{\partial \sigma} \textcircled{3} + S_\sigma \textcircled{4} - D_\sigma \textcircled{5} \quad (2)$$

In Eq. (2), $p^* = p_s - p_t$; p_s and p_t are the surface pressure and the pressure at the top of model atmosphere, respectively. The implication of each term in Eq. (2) is that, term ① is the tendency of sand-dust concentration with weight p^* ; terms ② and ③ are the horizontal and vertical flux transports of sand-dust with weight p^* , respectively; and terms ④ and ⑤ are source and sink terms of sand-dust, respectively, in σ coordinate system.

2. Parameterization of the Sand-Dust Source (Mobilization) Term

Based on the synoptic conditions for the formation of both the black storm and the sand-dust storm, the source term S_σ of the sand-dust should be related to the L_d category of the underlying surface, the density ρ_d of the soil and material at the ground, the wind velocity V_S near the ground, and the distance $V_S \Delta t$ of the wind erosion ground in time Δt and the suffered shearing stress τ_s in unit area at the surface. Thus the sand-dust source term can be parameterized by the following formula

$$S_\sigma = (V_S^2 \Delta t) \left(\frac{\tau_s}{\Delta S} \right) \rho_d L_d \quad (3)$$

When considering the following relations in the surface layer,

$$\tau_s = \rho_s u_*^2, \quad V_S = \left\{ \frac{1}{\kappa} \ln \left(\frac{z_S}{z_0} \right) - \Psi_m \left(\frac{z_S}{L} \right) \right\} u_* = A_0 u_*$$

Eq. (3) can be expressed as

$$S_\sigma = L_d \left[a_0 \left(\frac{\Delta t}{\Delta S} \right) (\rho_s \rho_d) \right] u_*^4 = L_d C_0 u_*^4, \quad (4)$$

where

$$C_0 = a_0 \left(\frac{\Delta t}{\Delta S} \right) (\rho_s \rho_d), \quad a_0 = A_0^2, \quad A_0 = \frac{1}{\kappa} \left[\ln \left(\frac{z_S}{z_0} \right) - \Psi_m \left(\frac{z_S}{L} \right) \right], \quad (5)$$

Δt is the integral time step, ΔS is the area of the model grid-mesh, ρ_s and ρ_d are the air density and sand-dust density near the ground, respectively, V_S is the wind velocity at z_S level, z_0 is the roughness. At the surface, Ψ_m is the stability parameter of momentum, L is M-O length, κ is Karman constant, u_* is the surface friction velocity, L_d is the coded number (non-dimension) of the categories for 13 underlying surfaces in the model, it represents the sand-dust underlying surface when $L_d = L_d(9)$; the $S_\sigma = 0$ when $L_d \neq L_d(9)$. Based on the analysis above, the source term S_σ of the sand-dust can be parameterized as follows:

$$S_\sigma = \begin{cases} 0, & u_* < u_{*c} \text{ or } q_{vs}(T_g) > q_c, \text{ or } L_d \neq L_d(9) \\ L_d C_0 u_*^4, & u_* \geq u_{*c} \text{ or } q_{vs}(T_g) \leq q_c, \text{ but } K_\sigma \neq 1, L_d = L_d(9) \end{cases} \quad (6)$$

where parameter C_0 is given in Eq. (5). $q_{vs}(T_g)$ is the saturated specific humidity near the ground. u_{*c} is the critical value of u_* ; Based on the analyzed results of wind speed for eight cases of the sand-dust storm in the western Saharan from 1 July to 15 August in 1974 by Helgren and Prospero (1988), we adopt the surface friction velocity critical value of $u_{*c} = 0.6 \text{ m s}^{-1}$ as the critical value of sand-dust mobilization at the ground; q_c is the critical value of $q_{vs}(T_g)$, which is 0.005 kg kg^{-1} ; K_σ is the number of vertical σ -level.

Besides, we here declare that the dimension of S_σ is consistent with those of other terms in Eq. (2). For example, in MKS ($\text{m} \cdot \text{kg} \cdot \text{s}$) system, the dimension of each term is the same, namely, $\text{M}^{-4}\text{K}^2\text{S}^{-3}$. For the S_σ related to C_0 , it is calculated only in the case of $L_d = L_d(9)$ which represents an underlying surface of the sand-dust material underlying surface. For example, $\kappa = 0.4$, $z_s = 1 \text{ m}$, $z_0(\text{desert}) = 3 \times 10^{-4} \text{ m}$, $\frac{z_s}{L} = -2$, thus $\ln \frac{z_s}{z_0} = 8.1017$, $\Psi_m\left(\frac{z_s}{L}\right) = 1.43$, where $\Psi_m\left(\frac{z_s}{L}\right) = -1.86\left(\frac{z_s}{L}\right) - 1.07\left(\frac{z_s}{L}\right)^2 - 0.249\left(\frac{z_s}{L}\right)^3$, it is the same as Ψ_m expressed in the case of the convective instability (Anthes et al. 1987); $A_0 = 16.68$, $a_0 = 278.2$; If $\Delta t = 90 \text{ s}$, $\Delta S = 1.6 \times 10^9 \text{ m}^2$, $\rho_s = 1.112 \text{ kg m}^{-3}$, $\rho_d = 1.5 \times 10 \text{ kg m}^{-3}$, we can get $C_0 = 0.0261 \text{ (m}^{-8} \text{ kg}^2 \text{ s)}$; When $u_* = 1 \text{ m s}^{-1}$, we can get S_σ from Eq. (6):

$$S_\sigma = L_d(9) (C_0 u_*^4) = (C_0 u_*^4) |_{\text{desert}} = 0.0261 \left(\frac{\text{kg}}{\text{m}^2 \text{ s}} \right) \left(\frac{\text{kg}}{\text{m s}^2} \right).$$

The result shows that the source term of the sand-dust in Eq. (2) will provide sand-dust at the rate of $26.1 \text{ g m}^{-2} \text{ s}^{-1}$ from the sand-dust underlying surface.

3. Parameterization of the Sand-Dust Sink (Sedimentation) Term

The sink term of the black storm means the process and the amount of the deposition at surface. Based on the physical intuition, it is proposed that the sink term of the sinking term of the sand-dust should be related to the concentration of sand-dust, the sand-dust weight in the air column above unit area, the dry deposition velocity of the sand-dust particles and the vertical velocity of air; Among them the sand-dust mass m_χ in the unit area air column is further related to the spatial distribution of the partial size spectrum of the sand-dust. Based on the consideration above, the parameterization of the sand-dust sink (sedimentation) term can be expressed as

$$D_\sigma = \chi \left(\frac{m_\chi g}{S_D} \right) (\dot{\sigma}_D + \dot{\sigma}_D'), \quad (7)$$

where $g = 9.8 \text{ m s}^{-2}$, it is the acceleration of gravity; the orders of magnitude for $\dot{\sigma}_D$ and $\dot{\sigma}_D'$ are both 10^{-5} s^{-1} in σ -coordinate system, m_χ is the function of the sand-dust particle size spatial distribution $n(z, r)$. Suppose the shape of the all sand-dust particles are ball, thus the sand-dust mass m_χ in the air column above unit area between z_1 - and z_2 -level can be calculated as follows:

$$m_\chi(z_1, z_2) = \frac{4}{3} \pi \rho_d \int_{z_1}^{z_2} \int_{r_1}^{r_2} r^3 n(z, r) dr dz, \quad (8)$$

where ρ_d is the density of dry sand, r is the radius of sand particle, $n(z, r) = A(z)n(r)$. Supposing the sand-dust particle size spatial distribution $n(z, r)$ obey the distribution of

Junge power function when the interval of the sand-dust particle radius is $0.15 \mu\text{m} \leq r \leq 10 \mu\text{m}$ and the depth of the sand-dust air layer is from ground to 1500 m. while we assume $A(z) = e^{-z/H}$ and divide both the sand-dust particle size spatial distribution of the black storm and the vertical level into three layers as follows:

$$\begin{cases} L_1: 0 \leq z \leq 500 \text{ m}, & 1 \mu\text{m} \leq r \leq 10 \mu\text{m}, & n(z, r) = e^{-z/H} C_1 r^{\gamma_1} \\ L_2: 500 \text{ m} < z \leq 1500 \text{ m}, & 0.15 \mu\text{m} \leq r \leq 1 \mu\text{m}, & n(z, r) = e^{-z/H} C_2 r^{\gamma_2} \\ L_3: z > 1500 \text{ m}. & r < 0.15 \mu\text{m} & n(z, r) = \text{const.} \end{cases} \quad (9)$$

Based on the observation and analysis of the aerosol particle size distribution in northern China by Zhu (1982), we adopted $C_1 = 25.75$, $\gamma_1 = 3.42$; $C_2 = 1.1383$, $\gamma_2 = 3.61$ and $H = 1500 \text{ m}$. The result of the sinking term calculated by this parameterization scheme will be given at Section V.

IV. DEVELOPMENT OF MESOSCALE NUMERICAL MODEL AND CONTROL SIMULATION

1. Addition of the Sand-Dust Transport Equation and the Development of MM4 Model

After adding the sand-dust transport Eq. (2) to the PSU/NCAR mesoscale numerical model (Anthes et al. 1987), and putting the horizontal and vertical diffusion terms in to Eq. (2), we get a set of equations as follows:

$$\begin{aligned} \frac{\partial p^* u}{\partial t} = & -m^2 \left(\frac{\partial p^* uu/m}{\partial x} + \frac{\partial p^* vu/m}{\partial y} \right) - \frac{\partial p^* \dot{\sigma} u}{\partial \sigma} \\ & - m p^* \left[\frac{RT_v}{(p^* + p_t/\sigma)} \frac{\partial p^*}{\partial x} + \frac{\partial \Phi}{\partial x} \right] + f p^* v + F_H(u) + F_V(u), \end{aligned} \quad (10)$$

$$\begin{aligned} \frac{\partial p^* v}{\partial t} = & -m^2 \left(\frac{\partial p^* vu/m}{\partial x} + \frac{\partial p^* vv/m}{\partial y} \right) - \frac{\partial p^* \dot{\sigma} v}{\partial \sigma} \\ & - m p^* \left[\frac{RT_v}{(p^* + p_t/\sigma)} \frac{\partial p^*}{\partial y} + \frac{\partial \Phi}{\partial y} \right] - f p^* u + F_H(v) + F_V(v), \end{aligned} \quad (11)$$

$$\frac{\partial p^*}{\partial t} = -m^2 \left(\frac{\partial p^* u/m}{\partial x} + \frac{\partial p^* v/m}{\partial y} \right) - \frac{\partial p^* \dot{\sigma}}{\partial \sigma} \quad (12)$$

$$\frac{\partial p^*}{\partial t} = -m^2 \int_0^1 \left(\frac{\partial p^* u/m}{\partial x} + \frac{\partial p^* v/m}{\partial y} \right) d\sigma \quad (13)$$

$$\dot{\sigma} = -\frac{1}{p^*} \int_1^\sigma \left[\frac{\partial p^*}{\partial t} + m^2 \left(\frac{\partial p^* u/m}{\partial x} + \frac{\partial p^* v/m}{\partial y} \right) \right] d\sigma, \quad (14)$$

$$\begin{aligned} \frac{\partial p^* T}{\partial t} = & -m^2 \left(\frac{\partial p^* uT/m}{\partial x} + \frac{\partial p^* vT/m}{\partial y} \right) - \frac{\partial p^* \dot{\sigma} T}{\partial \sigma} \\ & + \frac{RT_v \omega}{C_{pm} (\sigma + p_t/p^*)} + \frac{\partial p^* Q}{C_{pm}} + F_H(T) + F_V(T), \end{aligned} \quad (15)$$

$$\omega = p^* \dot{\sigma} + \sigma \frac{dp^*}{dt}. \quad (16)$$

$$\frac{dp^*}{dt} = \frac{\partial p^*}{\partial t} + m \left(u \frac{\partial p^*}{\partial x} + v \frac{\partial p^*}{\partial y} \right). \quad (17)$$

$$\frac{\partial \Phi}{\partial \ln(\sigma + p_t/p^*)} = -RT_v \left(1 + \frac{q_c + q_r}{1 + q_v} \right)^{-1}, \quad (18)$$

$$\frac{\partial p^* \chi}{\partial t} = -m^2 \left(\frac{\partial p^* u\chi/m}{\partial x} + \frac{\partial p^* v\chi/m}{\partial y} \right)$$

$$-\frac{\partial p^* \sigma \chi}{\partial \sigma} + F_H(\chi) + F_V(\chi) + S_\sigma - D_\sigma. \quad (19)$$

The description for further details of Eqs. (10) – (18) may refer Anthes et al. (1987). Equation (19) of the mobilizing and transporting sand-dust is added by author, in which $F_H(\chi)$ and $F_V(\chi)$ are the horizontal and vertical diffusion terms of the sand-dust concentration, respectively; S_σ and D_σ are the parameterized formulas of the sand-dust source and sink terms, respectively, which were given in Eqs. (6) and (7), respectively. The horizontal diffusion of the sand-dust concentration was calculated by fourth order difference scheme (Anthes et al. 1987):

$$F_H(\chi) = p^* K'_H \nabla^4 \chi, \quad K'_H = (d)^2 K_H, \\ K_H = A \left(K_{H0} + \frac{1}{2} \kappa^2 d^2 D \right), \quad (20)$$

where κ is Karman constant, D is the horizontal deformation, d is horizontal grid spacing, K_{H0} is the background value of K_H , A is the amplitude factor used to increase horizontal diffusivity.

The calculation of the sand-dust vertical diffusion term was based on K-theory:

$$F_V(\chi) = p^* K_z \frac{\partial^2 \chi}{\partial z^2}, \quad (21)$$

where the vertical diffusion K_z is the function of local R_i number. According to Anthes et al. (1987), it can be expressed as

$$K_z = \begin{cases} K_{z0} + l^2 S^{\frac{1}{2}} \frac{Ric - Ri}{Ric}, & \text{for } Ri < Ric \\ K_{z0}, & \text{for } Ri \geq Ric \end{cases} \quad (22)$$

where $K_{z0} = 1.0 \text{ m}^2 \text{ s}^{-1}$, Ric is the critical Ri ($R_i = \frac{g}{S\theta} \frac{\partial \theta}{\partial z}$, $S = \left(\frac{\partial u}{\partial z} \right)^2 + \left(\frac{\partial v}{\partial z} \right)^2 + 10^{-9}$) number, the added term 10^{-9} is to avoid Ri approaches infinity when the vertical shearing of wind comes to zero.

2. Control Simulation

(1) Basic model parameters: The constant pressure of the top of the model: $p_t = 100$ hPa; the number of the levels vertically: $K_\sigma = 16$; the horizontal grid spacing: $d = 40$ km; the center of computational domain: $C = 38^\circ\text{N}, 103^\circ\text{E}$; the computational horizontal domain contains an array of grid points: $N = 46 \times 61$.

(2) Initial condition: Chinese NMC (T_{42}) global analysis + sounding data.

(3) Lateral boundary condition: The time-dependent sponge boundary, the large scale tendency is obtained by linearly interpolating the 12-h analyses in time.

(4) Planetary boundary layer (PBL) physical process: Blackadar's high resolution PBL parameterization.

(5) Surface physical process: Including surface heat flux, moisture flux and momentum flux at the inhomogeneous surface.

(6) Ground temperature: It is predicted from a slab model and a surface energy budget including cloud effect, in which the radiate fluxes depend on the model predicted.

(7) Cumulus convective parameterization: Adopting Anthes-Kuo's scheme.

(8) Model topography: The terrain of the grid points for 40 km grid spacing is

obtained by analyzing the NCAR 0.5° terrain data through using mesoscale objective analysis scheme.

(9) Landuse categories: Through analyzing the global landuse data and dividing the data into 13 categories representing ground character, while the some physical parameters for the desert were revised by HEIFE data.

(10) Parameterization of the sand-dust: a sand-dust transport equation including parameterized terms of driving the sand-dust mobilization from the surface and the downward sedimentation of the sand-dust is proposed.

(11) Initial concentration field of the sand-dust: Horizontal uniform concentration field of the sand-dust.

(12) Projection time of the simulation: 24 h, namely, from 2000 BT 4 May to 2000 BT 5 May 1993.

The control simulation included all of the conditions and the processes as mentioned above. Next we will discuss the results of the simulation of the "93.5" black storm.

V. NUMERICAL SIMULATED RESULTS AND DISCUSSION

Figure 4 is the simulated 700 hPa vorticity field after 21 h from initial time 2000 BT 4 May 1993. We can see from the simulated results of each three hours output, the forming and developing process of this black storm was basically reproduced. In the 700 hPa vorticity field after integrating 18 h (figure omitted), a vorticity center of $48.27 \times 10^{-5} \text{ s}^{-1}$ was formed at the west of Jinchang. This vortex developed area was corresponding to an intensive allobaric gradient convergence zone on the both sides of the surface cold front

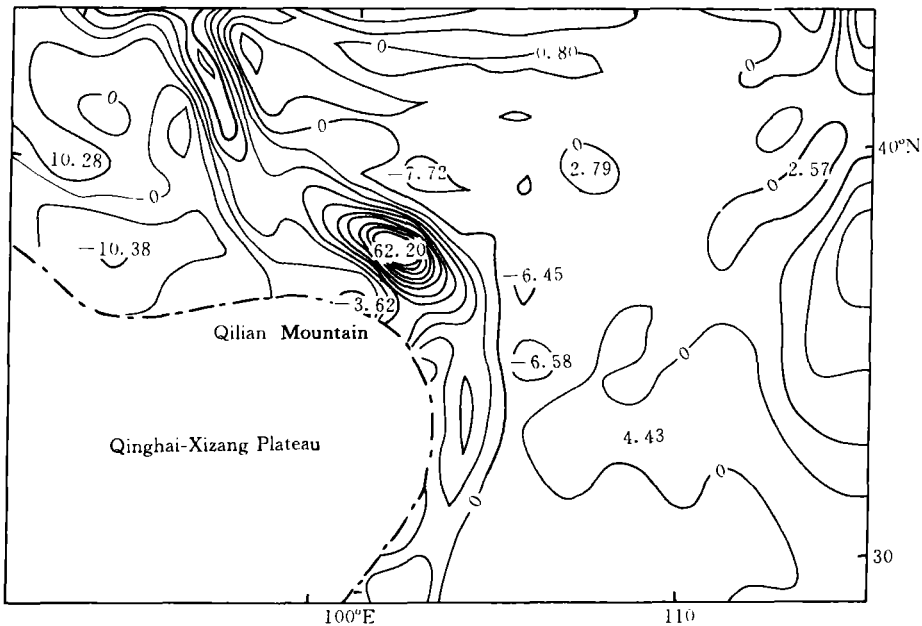


Fig. 4. The simulated 700 hPa vorticity field from control simulation after 21 h integration (verifying at 1700 BT 5 May 1993). The contour interval for vorticity is $5 \times 10^{-5} \text{ s}^{-1}$, the heavy dot-dashed line indicates the 3000 m terrain contour, ▲ represents Jinchang).

(figure omitted). Three hours later, namely 1700 BT, the mesoscale vortex moved eastward and continued to develop intensely (Fig. 4), the intensity of its vorticity center reached $62.20 \times 10^{-5} \text{ s}^{-1}$. This simulated result is consistent and synchronous with the genesis and intensive development of the black storm. moreover, the area of intensive developed vortex is basically consistent with the observed black storm area (Fig. 1). Just as pointed out in reference (Cheng and Ma 1996), the development and movement of the black storm was closely related to the development of this vortex. Figure 5 presents the W-E vertical cross section through the vorticity center of the vortex in Fig. 4. we can see that an intense cyclonic vorticity column stretched from the surface to 400 hPa near Jinchang while just superposing over it, an anticyclonic vorticity column stretched up to tropopause. The dynamical characteristic of such vortex column structure is that there is the intensive convergence inflow and corresponding strong ascending motion within the column at lower levels, while there is the intense divergence outflow and corresponding asymmetric descending motion around the column at upper levels. As a consequence, the intense ascending motion in vortex column of the black storm was driven to develop continuously and the wind at surface was also strengthened. Furthermore, the thermodynamical structure of the vortex column led to a strong convective at lower level. Such dynamical and thermodynamical structures are extremely favorable for the development of the black storm.

Figure 6 shows the screen-level horizontal distribution of the sand-dust concentration at 21 h from the initial time in the control simulation. The results in Fig. 6 were simulated by the MM4 model with inclusion of the sand-dust transport Eq. (2). We found that the maximum sand-dust concentration center is 1179 mg m^{-3} near Jinchang, this value is quite close to the observed sand-dust concentration 1016 mg m^{-3} at 1630 BT 5 May 1993 at Jinchang (Chen et al. 1993). The maximum sand-dust concentration is decreased to 679.1 mg m^{-3} (figure omitted) at the end of the 24-h simulation, in the mean time, the black storm event was approaching the end.

Figure 7 presents the west-east vertical cross section of the concentration through the maximum sand-dust concentration center in Fig. 6. The black storm was the severest at that time, and the sand-dust was vertically transported up to 700 hPa. Figure 8 gives the trajectories of some sand-dust particles during the 24-h period of simulation. We can see that most particles moved from Badain Jaran Desert to Tengger Desert in the northwest-southeast direction, and the others moved towards northeast.

Figure 9 shows the contours of the accumulated sand-dust deposition amount at the ground during the first 21-h of simulation. It is shown that the area of the sand-dust sedimentation was wider than the area of the sand-dust concentration field near the ground in Fig. 6 and the main center of the sand-dust sedimentation was located behind the center of the sand-dust concentration near the ground. Based on estimating from the center of the maximum sand-dust sedimentation, the sand-dust sedimentary rate is $15 \text{ g m}^{-2} \text{ s}^{-1}$, which is smaller than the sand-dust mobilizing rate $26.19 \text{ g m}^{-2} \text{ s}^{-1}$ from the ground. Obviously, the difference between the rate of the sedimentation and the mobilization was due to the fact that some sand-dust was diffused vertically to upper-air and transported horizontally to distant areas.

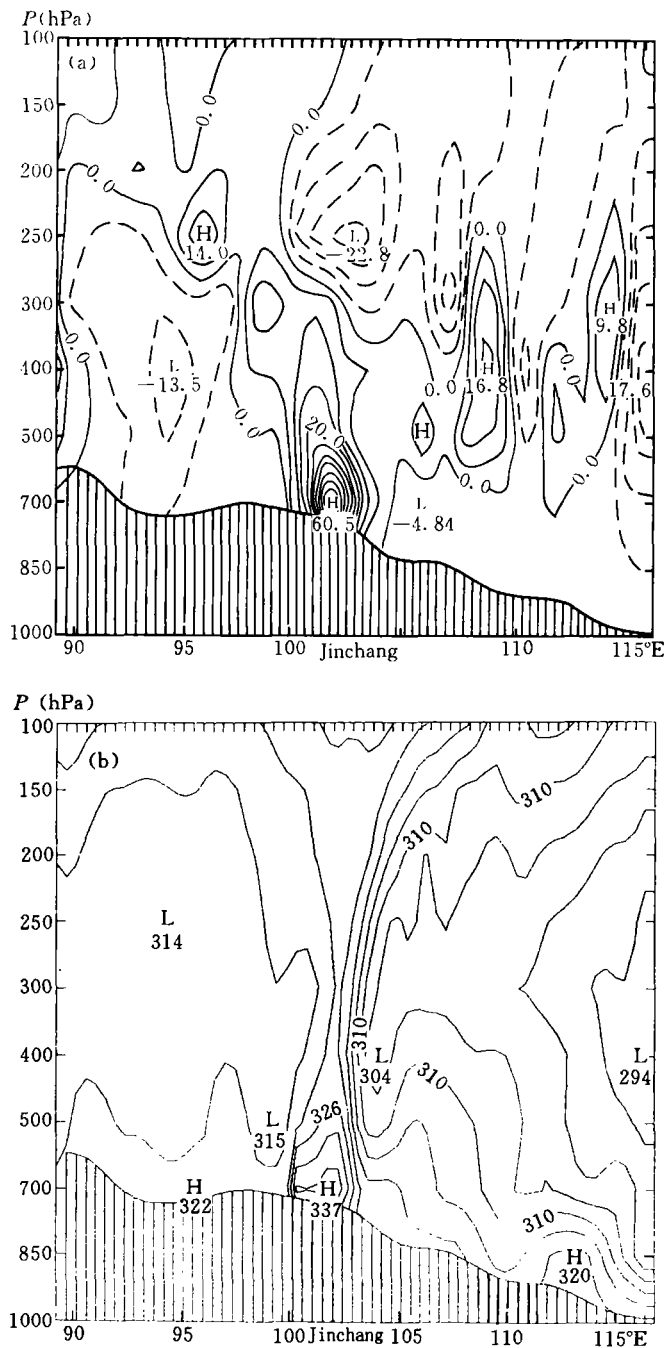


Fig. 5. The west-east vertical cross section of (a) vorticity ($5 \times 10^{-5} \text{ s}^{-1}$) and (b) equivalent potential temperature (K) through the vorticity center (Fig. 4) near Jinchang.

As for the simulation of the "April 1994" sand-dust storm, the similar results were obtained except that the time range for simulation was 36 h. It will not be discussed here because of the page limitation of the article.

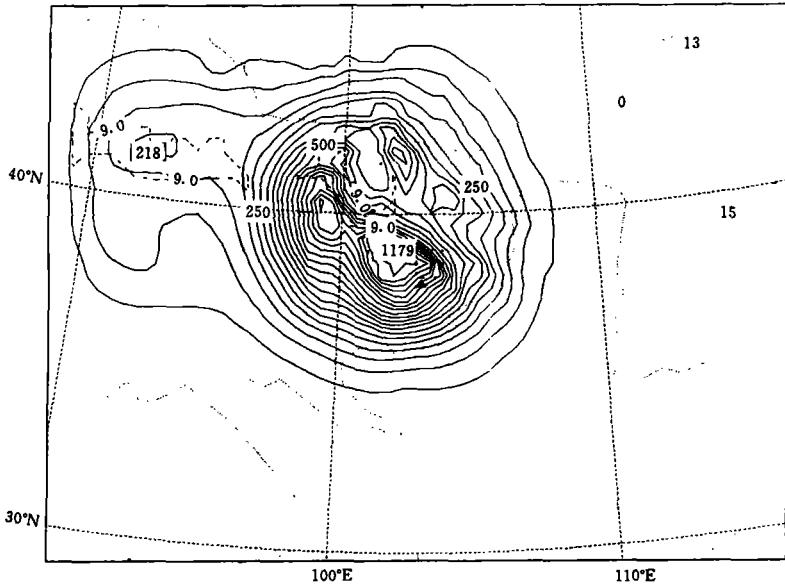


Fig. 6. The simulated screen-level horizontal field of the sand-dust concentration from the control simulation after 21 h integration (verifying at 1700 BT 5 May 1993; The contour interval for concentration is 50 mg m⁻³, ▲ represents Jinchang).

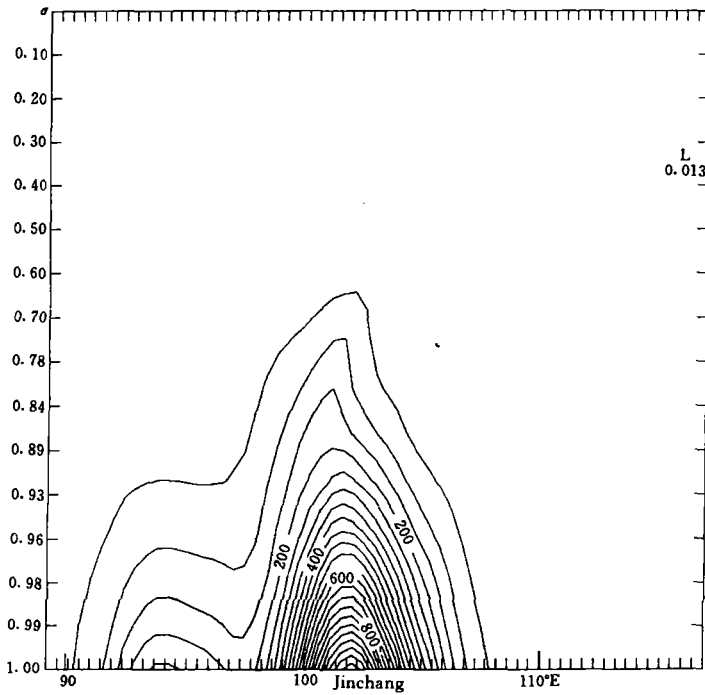


Fig. 7. The west-east vertical cross section of the concentration through the maximum sand-dust concentration center in Fig. 6.

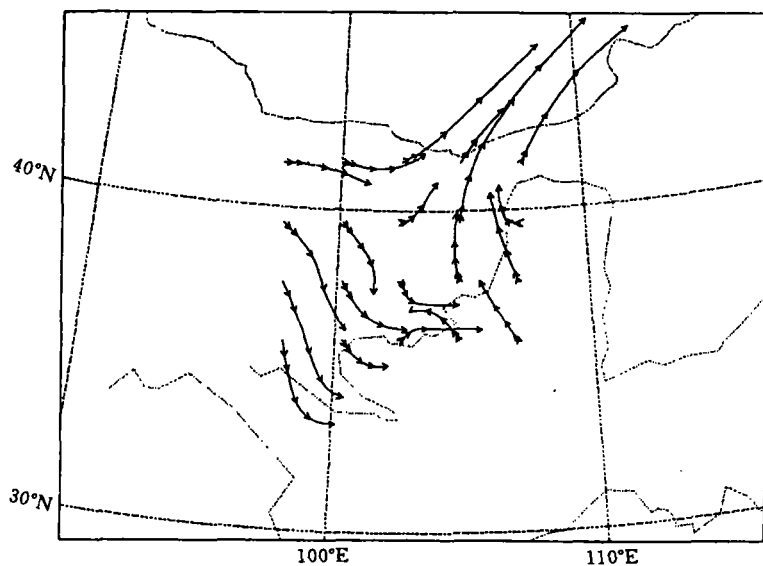


Fig. 8. The trajectories of the some sand-dust particles during the 24-h period of simulation.

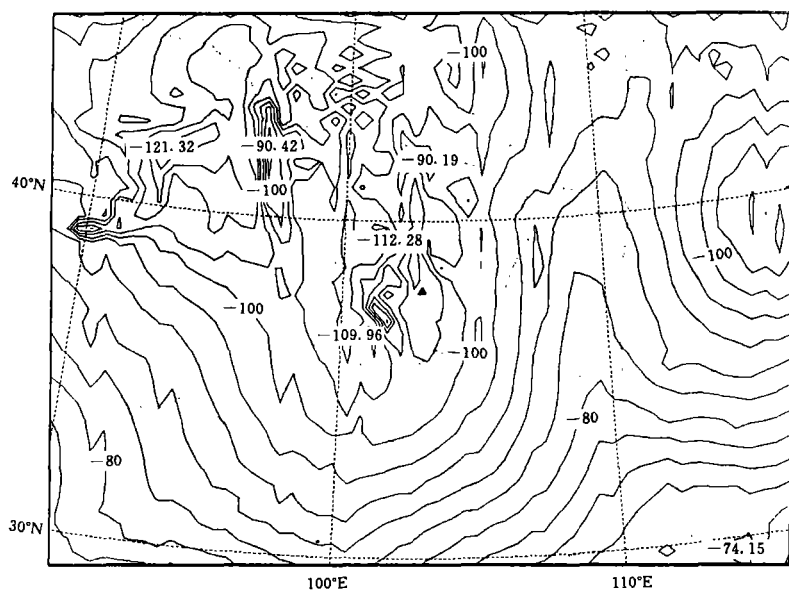


Fig. 9. The contours of the accumulated sand-dust deposition amount at the ground during the the first 21-h of the control simulation (The contour interval for the amount is 4 kg m^{-2}).

VI. CONCLUSIONS

Based on the analysis and discussion concerning the results of mesoscale numerical simulation, we draw the conclusions as follows:

(1) The synoptic analysis indicated that the typical black storm or sand-dust storms in the northwestern China are generated and developed through an interaction between the specific large scale circulation pattern and mesoscale systems. The passing by/over a huge sand-abundant desert of a strong cold front with intensive frontal zone at mid and lower levels is a necessary condition for the formation and development of a black storm or a severe sand-dust storm, and the presence of instability also provides an important thermodynamical condition for their development. A typical black storm like that occurring in May 1993 possesses some characteristics of a squall line.

(2) The results of the control simulation showed that a mesoscale model with a relative complete package of physics, high spatial resolution and a sufficient large simulation domain is able to simulate successfully the genesis and development of the mesoscale weather systems associated with the black storm, though the simulation was initialized with the conventional observation data whose spatial resolution is relative low.

(3) The results also revealed that the modified MM4 model, with inclusion of a dust transport equation and a parameterization of the dust source-sink terms, was able to simulate successfully the mobilization, transport and sedimentation of the dust in the "May 1993" and "April 1994" cases. For both cases, the simulated horizontal distributions of the dust concentration at screen level were roughly consistent with the observation.

(4) It is necessary to set up a field observational experiment of the sand-dust storms so as to obtain the concentration data of the sand-dust distribution in the space and the data of environmental field and structural evolution of the black storms and the sand-dust storms. These data are significant for further developing a parameterized scheme of the mobilization and transport of the sand-dust as well as the mesoscale model and simulation. It is also quite necessary to establish and develop a short-term forecasting system for the black storms and the sand-dust storms.

REFERENCES

- Anthes, R. A., Hsie, E. Y. and Kuo, Y. H. (1987). Description of the Penn State/NCAR Mesoscale Model Version 4 (MM4). NCAR TECH. Note, NCAR/TN-282+STR, pp. 66
- Cheng Linsheng, Ma Yan and Liu Chuntao (1995). Influence of mesoscale model resolution on the evaluative simulation of the "93. 5" black storm. *International Workshop on Limited-Area and Variable Resolution Models* (23-27 October 1995, Beijing). WMO/TD. No. 699: 323-328.
- Cheng Linsheng and Ma Yan (1996). The developing structure of a black storm and its numerical experiment of different model resolution. *Quart. J. Appl. Meteor.*, 7: 385-395 (in Chinese).
- Chen Minlian, Guo Qingtai and Xu Jianfen (1993). Study of the black storm weather. *Gansu Meteorology*, 11 (3): 16-27 (in Chinese).
- Helgren, D. M. and Prospero, J. M. (1988). Wind velocity associate with dust deflation events in the western Sahara. *J. Clim. Appl. Meteor.*, 26: 1147-1151.
- Huang Shizhu (1994). Seldom "yellow rain" weather. *Gansu Meteorology*, 12 (2): 16-21 (in Chinese).
- Iwasaka, Y. H., Minoura and Nagaya, K. (1983). The transport and special scale of Asian dust storm clouds: a case study of the dust storm event of April. *Tellus*, 35B (3): 189-196.
- Jiang Jixi (1995). A study of formation for "black storm" using GMS-4 imagery. *Quart. J. Appl. Meteor.*, 6: 177-184 (in Chinese).
- Karyampudi, V. M. and Carlson, T. N. (1988). Analysis and numerical simulation of the Saharan air layer and its effect on easterly wave disturbances. *J. Atmos. Sci.*, 45: 3102-3136.

- Westphal, D. L., Toon, O. B. and Carlson, T. N. (1988), A case study of mobilization and transport of Saharan dust, *J. Atmos. Sci.*, **45**: 2145—2175.
- Xu Jianfeng (1996), Study of the "94. 4" sand dust storm in Northwest of China, *China Desert*, **16**: 281—286 (in Chinese).
- Xu Guochang, Che Minglian and Wu Guoxiong (1979), Analysis of the "4. 22" severe sand-dust storm in Gansu Province, *Acta Meteor. Sinica*, **37**: 26—35 (in Chinese).
- Yang Gengsheng, Wang Yimao and Zhao Xingliang (1993), The endangering and countermeasures of the "5. 5" black storm in Northwest of China (in Chinese), *Gansu Meteorology*, **11** (3): 43—48 (in Chinese).
- Zhu Wenqin (1982), Observational analysis of aerosol size distribution, *Chinese J. Atmos. Sci.*, **6**: 217—223 (in Chinese).